Quantification of Fluorophore Copy Number from Intrinsic Fluctuations during Fluorescence Photobleaching

Chitra R. Nayak and Andrew D. Rutenberg*
Department of Physics and Atmospheric Science, Dalhousie University, Halifax, Nova Scotia, Canada

ABSTRACT We present a theoretical technique for quantifying the cellular copy-number of fluorophores that relies on the random nature of the photobleaching process. Our approach does not require single-molecule sensitivity, and therefore can be used with commonly used epifluorescence microscopes. Fluctuations arising from photobleaching can be used to estimate the proportionality between fluorescence intensity and copy-number, which can then be used with subsequent intensity measurements to estimate copy-number. We calculate the statistical errors of our approach and verify them with stochastic simulations. By using fluctuations over the entire photobleaching process, we obtain significantly smaller errors than previous approaches that have used fluctuations arising from cytoplasmic proteins partitioning during cellular division. From the time-dependence of the fluctuations as photobleaching proceeds, we can discriminate between desired photobleach fluctuations and background noise or photon shot noise. Our approach does not require cellular division and the photobleaching rate sets a timescale that is adjustable with respect to cellular processes. We hope that our approach will now be applied experimentally.

INTRODUCTION

Absolute quantification of the number of various proteins within a cell is important for quantitative biology, because expression number controls both nonlinear interactions and noise and is an important variable in quantitative modeling. The average expression number of a particular protein is an easily controlled experimental parameter through the use of inducible promoters. However, traditional immunoassay techniques for protein quantification are slow, ex vivo, and can have large variability (1). Several quantification techniques use microscopy of fluorescently tagged proteins, but still have limitations. Total-internal reflection fluorescence techniques allow for direct counting of protein subunits (2,3) but do not have the depth of field to allow for whole-cell quantification. Fluctuation correlation spectroscopy (FCS) and its refinements (4) allow for local density measurements using confocal microscopes, but only of freely diffusing proteins. Photoactivatable fluorophores allow for whole-cell counting (5), but the counting remains slow and require single-molecule sensitivity.

It is appealing to quantify fluorescently labeled proteins in vivo using their total cellular fluorescence. Fluorescence microscopy can characterize cell-by-cell variations of protein expression (6) as well as time-dependent fluctuations of protein expression for individual cells (7). However, the brightness of calibration standards may depend upon their environment (1) and the use of internal standards (8,9) is laborious. A promising recent approach is to calibrate the fluorescence signal against the intrinsic fluctuations that occurs during partitioning of cytoplasmic fluorescently labeled proteins upon cellular division (10,11). However, this division-fluctuation approach is limited to freely diffusing cytoplasmic proteins in cells, such as bacteria, of simple geometry that are also actively dividing. Because many interesting proteins are localized to membranes (12), and not all cells are actively dividing, it would be useful to reduce these restrictions.

As we will detail in our theoretical study, the random photobleaching of individual fluorophores can, in principle, provide intrinsic fluctuations with which we can quantify fluorescently labeled proteins within a cell. These fluctuations are easily resolvable by epifluorescence microscopy (10,11) even where individual photobleaching events are not. Photobleaching is a random process by which fluorescent molecules undergo a light-induced chemical transformation and lose the ability to fluoresce. Most simply, the average number of unbleached fluorophores will decay as $\exp(-t/\tau)$—characterized by a timescale τ that is inversely dependent on the illumination intensity. An appropriate ensemble of cells would have, on the timescale of photobleaching, similar internal environments. Because of its cagelike design (13), standard green fluorescent protein (GFP) variants are thought to be relatively insensitive to their environment (14), though environmental photobleach sensitivity to oxygen (15,16) and to variations of pH (17) is observed.

Although using fluctuations for quantification is appealing, accuracy can be affected by undesired fluctuations arising from photon shot noise, fluorescent-protein synthesis and degradation, cell motion into or out of the focal volume, and instrumental noise. Inadvertently adding these fluctuations into the quantification analysis will generically lead to a systematic underestimate of expression numbers. We address this in two ways, which should provide guidance for experimental implementation of our

Submitted March 15, 2011, and accepted for publication September 21, 2011.

*Correspondence: adr@dal.ca or andrew.rutenberg@dal.ca

Editor: Catherine A. Royer.

0006-3495/11/11/2284/10 $2.00

doi: 10.1016/j.bpj.2011.09.032

approach: 1), We show how the photobleach fluctuations evolve in time and how they depend on illumination intensity—so that the time-dependence and illumination-dependence of the fluctuations can be used to validate the desired fluctuations. 2), We calculate the expected quantification errors due to the photobleaching stochasticity. This provides a consistency check against the experimentally estimated quantification error. Using this, we can show that earlier studies of division-fluctuation quantification (10) had significant bias, but more recent studies (11) did not. Notwithstanding, photobleach fluctuations provide more information per cell than division-fluctuations.

QUANTIFICATION FROM PHOTOBLEACH FLUCTUATIONS

The spatially integrated background-subtracted fluorescence intensity I from one cell will be proportional to the number of fluorophores n in the cell,

$$I = \nu n. \tag{1}$$

If we measure the intensity as the number of fluorescent photons collected in a time-interval Δt and if ψ_{ex} is the excitation (illumination) intensity, then $\nu \propto \psi_{ex}\Delta t$, where the proportionality constant includes details of both the particular fluorophore and of the optics.

The number of active fluorophores will decrease due to irreversible photobleaching. The probability $P(n,t)$ that n fluorophores out of the original n_0 have avoided photobleaching at time t is given by the binomial distribution,

$$P(n,t) = \frac{n_0!}{n!(n_0-n)!}p^n(1-p)^{n_0-n}, \tag{2}$$

where p is the average fraction of surviving fluorophores at time t. We expect $p = \exp(-t/\tau)$, corresponding to cells under constant and uniform illumination.

To illustrate the stochastic fluctuations in Fig. 1, we have simulated a random photobleach process with the exact Gillespie algorithm (18), with time measured in units of τ. The thick-black line of the log-lin plot shows the deterministic average, $n_0 \exp(-t/\tau)$, whereas the thinner blue lines show 25 independent photobleach curves each starting with the initial number of fluorophores $n_0 = 500$ (a typical expression level of bacterial proteins (19)). The magnitude of fluctuations is time-varying—vanishing at $t = 0$ when no bleaching has yet occurred and again as $t \to \infty$ when all fluorophores are bleached. In the inset we show that best-fit exponential timescales are appreciably scattered around the actual $\tau = 1$. (Least-squares fits assume uncorrelated fluctuations of, e.g., photoemission lifetimes (20).) In contrast, the stochastic intensity decay $I(t)$ has strong autocorrelations (for example, see the *thin blue lines* in Fig. 1), and do not give precise fits. As a result, we need to average

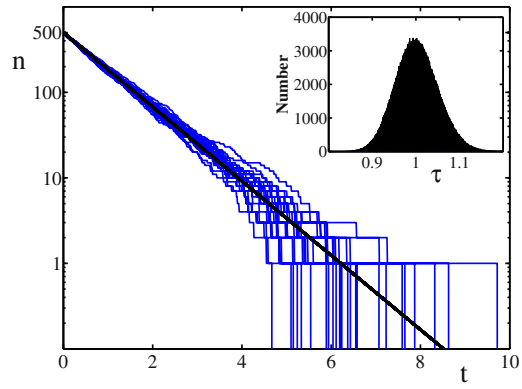

FIGURE 1 (*Thin blue lines*) Twenty-five independent stochastic photobleaching curves from $n_0 = 500$ initial fluorophores with lifetime $\tau = 1$, from exact numerical simulations. The number of unbleached fluorophores n are plotted versus time t. (*Solid line*) Deterministic average, $n_0 \exp(-t/\tau)$. The time-dependent magnitude and the nonzero autocorrelations of the photobleach fluctuations are apparent. (*Inset*) Distribution of the best-fit lifetimes τ (10^6 samples over 1000 bins) for naive least-squares fits to the stochastic curves, showing significant variation.

the photobleach decay curves from an ensemble of cells to determine p and thereby determine fluctuations using the initial intensity $I(0)$.

Given an initial number of fluorophores n_0 in a cell, with $n(t)$ remaining fluorophores at time t, then the average $\langle n\rangle = pn_0$ and the variance of n follows from the binomial distribution Eq. 2:

$$\sigma_n^2 \equiv \left\langle (n-\langle n\rangle)^2\right\rangle = \left\langle n^2\right\rangle - \left\langle n^2\right\rangle = p(1-p)n_0. \tag{3}$$

The variance of the measured fluorescence intensity $I(t) = \nu n$ is then

$$\sigma_I^2 \equiv \left\langle (I-\langle I\rangle)^2\right\rangle = \nu^2\sigma_n^2 = I_0\nu p(1-p), \tag{4}$$

where $I_0 \equiv I(0) = \nu n_0$. As a function of the photobleached fraction $1-p$, which is a timelike variable that increases with time from 0 to 1, the intensity variance follows a symmetric parabola that is peaked at $p = 1/2$—where maximal photobleach fluctuations are seen. This is illustrated by the parabolic dashed black line in Fig. 2. We also show exact numerical simulations, using the Gillespie algorithm (18), of the average variance seen from $n_0 = 100$ initial fluorophores (*solid red lines*). We show three independent averages of $M = 100$, where M is the number of samples (i.e., the number of cells or bacteria). Although the average variances versus $1-p$ are approximately parabolic, and do recover the analytic result as $M \to \infty$ (data not shown), we also notice significant variations due to the finite sample size M. These variations will lead to a nonzero variance of our estimation of ν, which we will calculate later.

We can use Eq. 4 to obtain ν, the intensity per fluorophore. We obtain

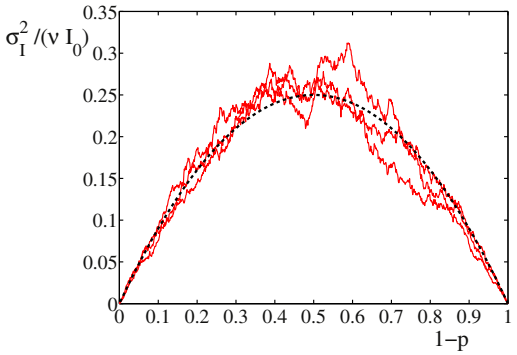

FIGURE 2 Scaled variance of the fluorescence intensity $\sigma^2_I/(\nu I_0)$ versus unbleached fraction $1-p$, where $p = \exp(-t/\tau)$. (*Dashed black line*) Parabolic average, from Eq. 4. (*Thin red curves*) Result of exact stochastic simulations of photobleaching $n_0 = 100$ initial fluorophores. Each curve is the average of the measured variance over $M = 100$ samples.

$$\nu = \frac{\sigma_I^2}{I_0 p(1-p)}, \tag{5}$$

as an unbiased estimate of ν from the fluctuations seen in a single cell at a given p. A sufficiently precise ν is then determined by averaging this estimate over many cells, which can thereafter be used to directly estimate n_0 from measured intensities. To minimize the single-cell variance, we can include the entire photobleach time-history by integrating both sides of Eq. 4 over p, as

$$\nu = 6\int_0^1 \frac{\sigma_I^2 dp}{I_0}, \tag{6}$$

where the result applies to a single-cell with initial integrated intensity I_0. Analogous expressions for ν from any particular subset or subrange of p values can be obtained by summing or integrating σ^2_I/I_0 from Eq. 4.

NATURAL ENSEMBLES OF CELLS

An experimental ensemble, or collection, of cells will have a distribution of expression levels $P_0(n_0)$ (19,21) and hence a distribution of initial fluorescence intensities $P_0(I_0)$. This can be approached in two ways. First, we could simply analyze the raw number variance over the experimental ensemble (see Appendix 1), obtaining

$$\sigma_n^2 = \sigma_{n_0}^2 p^2 + \langle n_0\rangle p(1-p). \tag{7}$$

We see that the variance due to the cellular expression, $\sigma^2_{n_0}$, is slowly reduced by photobleaching while the additional variance due to photobleaching itself has the characteristic quadratic dependence on p. In terms of intensities, this gives

$$\sigma_I^2 = \sigma_{I0}^2 p^2 + \langle I\rangle_0 p(1-p)\nu, \tag{8}$$

where the subscript 0 indicates $t = 0$.

Alternatively, Eq. 6 represents an unbiased estimate of ν for an individual cell if I_0 is the corresponding initial intensity of that same cell. We can then simply average the resulting single-cell estimates of ν over the ensemble of cells, even if I_0 varies appreciably from cell to cell. As we shall see below, for $n_0 \gtrsim 10$ the variances of ν are approximately independent of n_0 and so an unweighted average of ν may be taken. This single-cell approach is used for the rest of this article.

VARIANCE OF ν DUE TO NUMBER OF FLUOROPHORES

At any given time, characterized by the surviving fraction p, the estimated ν from Eq. 5 from a given individual cell is given by

$$\nu_p \equiv \frac{\nu^2(n-\langle n\rangle)^2}{(I_0 p(1-p))} = \frac{\nu(n-pn_0)^2}{(n_0 p(1-p))}.$$

The variance of these estimates is then

$$\sigma^2_{\nu_p} = \left\langle \left(\nu_p - \nu\right)^2\right\rangle, \tag{9}$$

$$= \frac{\nu^2\left\langle (n-pn_0)^4\right\rangle}{p^2(1-p)^2 n_0^2} - \nu^2, \tag{10}$$

$$= \nu^2\left[2 - \frac{6}{n_0} + \frac{1}{n_0 p(1-p)}\right], \tag{11}$$

where we have used the moments of the binomial distribution, Eq. 2, to get the last line. For $p = 1/2$, which applies to binary division studies (10,11), this gives $\sigma^2_{\nu_{1/2}} = 2\nu^2(1 - 1/n_0)$. The variance can be used for weighted averages of estimates of ν from an ensemble of bacteria with different initial n_0—but in practice, equally weighted averages of ν can be taken as long as $n_0 \gtrsim 10$.

There is additional information to be obtained by considering the entire photobleaching curve as in Eq. 6. Although autocorrelations make the calculation of the variance of the estimated ν slightly more involved (see Appendix 2), the result is simply

$$\sigma^2_\nu = \nu^2\left(\frac{4}{5} - \frac{3}{5n_0}\right). \tag{12}$$

In the large n_0 limit, variances are approximately half as large when the entire photobleaching curve is used to estimate ν. We have plotted both $\sigma^2_{\nu_{1/2}}/\nu^2$ and σ^2_ν/ν^2 in Fig. 3. The corresponding numerically determined variance of the ν estimates, from 10^6 single-cell samples starting at each n_0 value and using exact stochastic Gillespie dynamics for the photobleaching, are plotted as points and coincide with our analytic expressions.

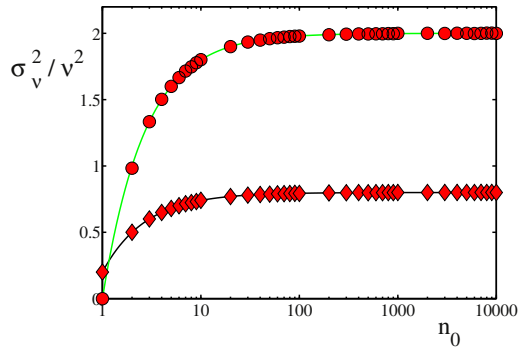

FIGURE 3 Scaled variance of single-cell estimates of ν, σ^2_ν/ν^2 versus the number of initial fluorophores n_0. The analytic variance for division-fluctuation with $p = 1/2$, $\sigma^2_{\nu_{1/2}}/\nu^2$ from Eq. 11, is shown (*green line*) together with numerical confirmation from 10^6 independent samples shown (*red circles*). The analytic variance for the integrated photobleaching, σ^2_ν/ν^2 from Eq. 12, is shown (*black line*) together with numerical confirmation from 10^6 independent samples shown (*red diamonds*). The relative error in ν from M samples is then $\sigma_\nu/(\nu\sqrt{M})$. For every $n_0 > 1$, the error is considerably less when the integrated photobleaching fluctuations are used.

To obtain the estimated error for ν due to fluctuation effects, where ν is the average result of measuring M cells, divide the standard-deviation σ_ν by $\sqrt{M}$. Now, consider fractional quantification error in division fluctuations (11) where the error due to fluctuations measuring M cells is $\delta n_0/n_0 = \delta\nu_{1/2}/\nu_{1/2} \approx \sqrt{2/M}$, because $n_0 \gtrsim 10$. Although photobleaching is not involved, $p \approx 1/2$ results from symmetric partitioning into two daughter cells. Using $M \approx 200$ cells (11), we obtain $\delta n_0/n_0 \approx 0.1$. This is approximately the experimentally reported fractional error (11), indicating systematic errors due to neglected sources of variance were not significant in that study. Conversely, an earlier division fluctuation approach that neglected slight asymmetries in cellular division (10) obtained a fractional accuracy $\delta n_0/n_0 \approx 0.27$ with $M \approx 700$ samples. This fractional error is significantly worse than the error due to fluctuations, which is $\sqrt{2/700} \approx 0.05$—implying that systematic errors, rather than intrinsic fluctuations, dominated the precision of that study.

VARIANCE OF ν DUE TO NUMBER OF CELLS

Our analysis assumes a precise estimate of the average photobleaching curve $\langle n\rangle = pn_0$. This is only achieved as the number of cells $M \to \infty$. For a finite ensemble of M cells, residual fluctuations in $\langle n\rangle$ will be correlated with individual samples. The result will be a systematic underestimate of the total fluctuations, and hence, ν. Fortunately, the effect is typically smaller than statistical errors and is both calculable and correctable.

The true time-dependent photobleach fluctuation of a cell i with respect to the average photobleaching curve is $\sigma_i(t) \equiv n_i - \langle n\rangle$. For a sample of M cells, we will estimate this with

$$\tilde{\sigma}_i \equiv n_i - \frac{1}{M}\sum_{j=1}^{M} n_j = \sigma_i\left(1-\frac{1}{M}\right) - \sum_j{}' \frac{\sigma_j}{M}, \tag{13}$$

where the primed sum indicates that $j = i$ is excluded. We use this to obtain

$$\left\langle \tilde{\sigma}^2 \right\rangle = \left\langle \sigma_i^2 \right\rangle \left(1-\frac{1}{M}\right)^2 + \sum_j{}' \frac{\left\langle \sigma_j^2 \right\rangle}{M^2} = \left\langle \sigma^2 \right\rangle \left(1-\frac{1}{M}\right), \tag{14}$$

because $\langle \sigma^2{}_i\rangle = \langle \sigma^2{}_j\rangle = \langle \sigma^2\rangle$. As expected, we naively underestimate fluctuations for any finite number of cells, which through Eq. 6 gives the same underestimate of ν (and overestimate of n_0). Knowing the number of cells M, we can simply correct for this effect by dividing the estimated variance by $1 - 1/M$.

We have numerically confirmed this systematic error due to a finite ensemble of cells in Fig. 4. The solid red line shows the expected behavior from Eq. 14, whereas the green points are the average ν_{est} from repeated simulations of ensembles of M cells. The error bars indicate the observed standard deviations of those repeated simulations—which characteristically decay as $1/\sqrt{M}$ for larger number of cells M. The corrected estimates are shown with black points, for $M \geq 1$, and are unbiased.

SYSTEMATIC ERRORS DUE TO NONPHOTOBLEACHING SOURCES OF VARIANCE

If they are not accounted for, nonphotobleaching sources of variance could affect quantification. Nonphotobleach

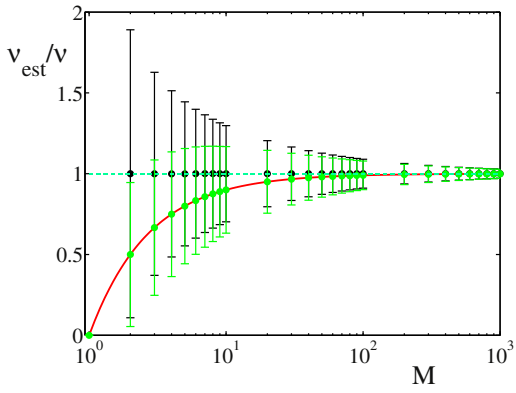

FIGURE 4 Ratio of the estimated to the actual value of ν, ν_{est}/ν, versus the number of cells M in a finite ensemble. (*Solid red line*) Predicted systematic error from Eq. 14. (*Green points*) Average results of 10^6 simulations of M cells each starting with $n_0 = 100$ fluorophores. Qualitatively identical results are found for larger n_0. The statistical errors shown are the measured standard deviations of the single-cell values of ν_{est}/ν. For $M > 1$, the systematic errors due to a finite number of cells M can be corrected with a multiplicative factor of $1/(1 - 1/M)$, from Eq. 14 (*black dots* and *error bars*).

fluctuations may be expected from photon shot noise, reversible photobleaching, cellular motion, and from ongoing fluorophore synthesis and/or degradation. The dominant source of fluctuations will depend upon the particular future experimental implementation. Any sources of variance that are not excluded from our fluctuation analysis will lead to an overestimate of photobleach fluctuations and to a quantification underestimate, because photobleach fluctuations increase with decreased expression. Fortunately, by considering the illumination-intensity dependence (via ψ_{ex}), the time-dependence (via p), and the exposure-time dependence (via Δt), we can theoretically differentiate the photobleach fluctuations from fluctuations due to shot-noise and cell-motion. By varying the illumination-intensity, we also vary the speed of photobleaching with respect to cellular motion, any physiologically controlled photophysical changes, and ongoing protein synthesis and degradation.

Shot-noise

Photon shot-noise, i.e., fluctuations due to variations in the number of photons emitted by the fluorophores, is a Poisson process with variance equal to its mean. Additional electronic shot noise in charge-coupled device (CCD) detectors will contribute similarly. We expect I photons to be received in a given exposure, so the variance of the number of photons received due to shot noise is $\sigma^2_{SN} = I = \nu p n_0$. By comparing this with photobleach fluctuations from Eq. 4, $\sigma^2_I = n_0 \nu^2\, p(1 - p)$, we see that shot noise has both a different time dependence (through p, decreasing as fluorophores are bleached) and a different illumination-intensity and exposure-time dependence (both through ν, increasing more slowly than photobleach fluctuations as brightness is increased), but the same dependence on n_0. Because typically the number of photons per fluorophore in an exposure is much more than one, i.e., $\nu >> 1$, we expect shot-noise to be a small effect (see illustrative workflow, below).

Other temporal variations of fluorophore brightness, such as blinking (22,23), will have the same statistics as shot-noise as long as the timescale of the collective variations is faster than the exposure-time Δt. Helpfully, the collective blinking rate of n fluorophores will be n times faster than the blinking of individual fluorophores.

Cellular motion

Motion of cells entirely within the field of view will not lead to variations of the fluorescence intensity. However, motion of parts of cells into or out of the imaging volume will lead to intensity fluctuations that are proportional to the fluorescence intensity I. The resulting variance will be proportional to the square-intensity, or $\sigma^2_{motion} \propto \nu^2 p^2$. The time-decay (via p) will be stronger than for shot-noise and distinct from photobleach fluctuations, though it has the same dependence on illumination intensity ψ_{ex} (via ν) as the variance due to photobleaching.

Ongoing protein translation

For genetically encoded fluorophores, such as green fluorescent protein (GFP), stochastic synthesis and/or proteolysis will lead to intensity fluctuations with temporal structure. Although proteolysis on its own simply modifies the effective photobleach lifetime τ, synthesis and subsequent fluorophore maturation are less straightforward. Nevertheless, if photobleaching is fast compared to synthesis, then the latter can be neglected (the photobleaching rate can be adjusted with the excitation intensity ψ_{ex}). If necessary, many short-duration bleaching experiments can be done, even on a single cell; i.e., for a range $p \in [p_{min}, 1]$ rather than $p \in [0, 1]$ as in Eq. 6.

Inhomogeneous illumination

Although inhomogeneous illumination does not lead to fluctuations per se, it does lead to a distribution of photobleach lifetimes (24,25) because the lifetime τ is inversely proportional to the illumination intensity. If significant, this must be corrected for by flattening the image (see, e.g., Taniguchi et al. (19)) before the ensemble average over cells is used to obtain $p(t)$.

Fluorescence anisotropy

Rigidly immobilized fluorophores have an anisotropic (dipole) emission intensity as well as an absorption cross section. Cytoplasmic fluorophores such as GFP typically rapidly rotationally diffuse (14). Even membrane-associated fluorophores will rotationally diffuse if the linker is sufficiently flexible (26). For rotational timescales much less than the photobleach timescale τ, anisotropy effects will be negligible. However, fluorophores that are rotationally immobilized will exhibit a broad range of photobleach lifetimes—and cannot be treated with our approach.

ILLUSTRATIVE WORKFLOW

Fig. 5 illustrates a simple workflow for estimating ν from a series of epifluorescence images. We use simulated data that include both photon shot noise from unbleached fluorophores as well as a constant Gaussian-distributed instrumental noise (see below). We use reasonable but illustrative values for our parameters (see below). In Fig. 5 *a*, we illustrate a portion of the field of view that includes several bacteria each expressing $n_0 = 100$ fluorophores. The bacteria are represented by ellipses (24 long, six pixels wide), and are cosmetically blurred with an isotropic Gaussian filter with a width of three pixels. We have indicated one region of interest, which includes one bacterium,

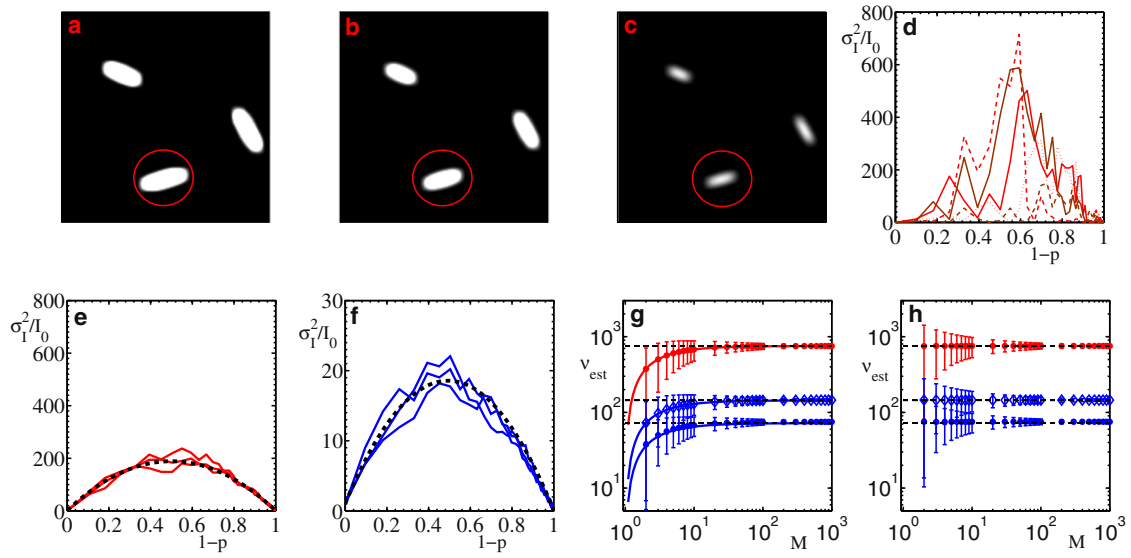

FIGURE 5 (*a–c*) Simulated field of view with region of interest (*red circle*, encompassing 452 pixels) surrounding one bacterium, at $t = 0$, $t/\tau = ln(2)$, and $t/\tau = ln(6)$. Each bacterium has $n_0 = 100$ fluorophores initially, with $\nu = 753$ (appropriate for EGFP with $\Delta t/\tau = 0.1$, see text) and Gaussian variance per pixel of $\sigma^2{}_G = 4$; (*d*) single-cell variances $\sigma^2{}_I/I_0$ for five cells versus $1 - p$, where $p = \exp(-t/\tau)$ is the fraction of unbleached fluorophores; (*e*) each trace (*red*) is the average of $M = 100$ single-cell variances, divided by the background-subtracted initial intensity I_0; (*f*) the same as panel *e* but with $\nu = 72$ (for R6G, see text); (*g*) estimated ν-values for ensembles of M cells from Eq. 6 using traces like those from panels *e* and *f*—the average and standard deviations are shown for $\nu =$ 753, 144, and 72 (*solid red circle*, *open blue circle*, and *solid blue circle*, respectively); and (*h*) same as panel *g* but corrected for the finite number of cells using Eq. 14. Only for very small ν (*solid blue circles*) are biases due to uncorrected shot-noise evident.

with a red circle. The summed pixel values within the region of interest is the raw integrated intensity $I_i(t)$ for cell i. We indicate two later frames of the same region in Fig. 5, *b* and *c*, at times $t/\tau = ln(2)$ and $ln(6)$, with approximately one-half and one-sixth of the original fluorophores, respectively.

Many such traces $I_i(t)$ would look similar to those in Fig. 1, and we can then take the average $\langle I\rangle \equiv \sum_{i=1}^{M} I_i(t)/M$, where there are M cells in the average. This average is then used to calculate the cell-by-cell variances $\sigma^2{}_{I,i}(t) \equiv (I_i - \langle I\rangle)^2$, five of which are illustrated in Fig. 5 *d*. The characteristic parabolic shape of the average variance is not yet immediately apparent in these single-cell unaveraged traces.

We model the raw observed intensity due to n fluorescent molecules as $I = \nu n + \eta_p + \eta_G + I_B$, where η_P is the random variation due to the Poisson-distributed photon shot noise with $\langle \eta_P\rangle = 0$ and $\sigma^2{}_{SN} \equiv \langle \eta^2{}_p\rangle = \nu n$, η_G is Gaussian-distributed instrumental noise with variance $\sigma^2{}_G \approx 4$ (27), and I_B is a constant instrumental offset that is removed by background subtraction. The total variance is then $\sigma^2_{tot} = \sigma^2_{PB} + \sigma^2_{SN} + \sigma^2_G$, where $\sigma^2{}_{PB}$ is from photobleach fluctuations as in Eq. 4. The commonly used EGFP will emit $n_\gamma = 251{,}000$ photons before photobleaching (17), whereas the easily bleached rhodamine 6G (R6G) will emit only $n_\gamma = 24{,}000$ (28). A small fraction $\alpha \approx 0.03$ of these photons will be detected by the CCD (27), due to considerations of solid-angle, lens surfaces, and detector efficiency. If the number of photons detected from a cell in a single frame is I_i, then the total over all frames is

$$\sum I_i = \sum \nu n_0 \exp\left(\frac{-t}{\tau}\right) \approx \int_0^\infty \nu n_0 \exp\left(\frac{-t}{\tau}\right)\frac{dt}{\Delta t} = \frac{\nu n_0 \tau}{\Delta t},$$

where Δt is the exposure duration. Equating this to $\alpha n_0 n_\gamma$ gives

$$\nu = \frac{\alpha n_\gamma \Delta t}{\tau}. \tag{15}$$

Because cells will typically have variable n_0 (19), we average $\sigma^2{}_I/I_0$—as in Eq. 6—and show the resulting average over ensembles of $M = 100$ cells in Fig. 5, *e* and *f*, together with the analytic average expected for $M = \infty$ with the dashed black lines. With a relatively long exposure, $\Delta t/\tau = 0.1$, we use Eq. 15 to obtain $\nu = 753$ for EGFP (17) (*red curves* in Fig. 5 *e*), and $\nu = 72$ for R6G (28) (*blue curves* in Fig. 5 *f*). The initial intensity I_0 is background-subtracted, to prevent biases due to instrumental offsets. Neither the Poisson shot-noise nor the Gaussian background are evident for the simulated EGFP data in Fig. 5 *e*. The simulated R6G data (Fig. 5 *f*) do show some shot-noise, evident in the nonzero value of $\sigma^2{}_I/I_0$ at $1 - p = 0$. For simplicity, we have taken this raw variance data, $\sigma^2{}_{tot}$, and with discrete trapezoidal integration, have calculated ν_{est} from Eq. 6 for ensembles of M cells. The resulting averages and standard deviations are indicated in Fig. 5 *g*, where the open blue circles are for R6G with $\Delta t/\tau = 0.2$, to reduce the relative impact of shot noise. To emphasize the error due to shot noise, we show ν_{est} corrected for finite M using Eq. 14 in Fig. 5 *h*. We see that only a slight bias can be seen for the

shorter exposures with R6G. With brighter fluorophores more resistant to bleaching, such as Mut2-GFP with $n_\gamma \approx 1.5 \times 10^6$ (29), we would anticipate even less error due to neglected shot-noise effects. Alternatively, large shot-noise effects can be characterized and corrected for.

Any epifluorescence microscope should be adequate in conjunction with a low-noise CCD and image analysis software to integrate regions of interest over stacks of frames. The effects of dark noise, or ${\sigma^2}_G$, is reduced with fewer pixels—i.e., at lower magnification. This also typically increases the number of cells, M, entirely within the field of view and the depth of field. We would suggest $M \gtrsim 100$, though any $M > 2$ is possible using the correction from Eq. 14. Longer exposures reduces the relative impact of shot-noise but we suggest $\Delta t/\tau \lesssim 0.1$, with at least 20 frames, to allow for convenient integration of Eq. 6 and to be able to control for nonphotobleaching sources of variance. The ensemble of cells can all have different n_0 values, as long as Eq. 6 is used for each. A large range of the number of fluorophores per cell, $n_0 \in [10,10^6]$, should be practical, depending on the dark noise of the imaging system at low n_0 and on the dynamic range of the region of interest at large n_0 (at least $\sqrt{n_0}$). Fluorophores that emit many photons, n_γ, before bleaching are best. Photoconversion, or other sources of nonexponential photobleaching, should be avoided.

SUMMARY AND DISCUSSION

In our theoretical study, we have shown how photobleach fluctuations could be used to quantify fluorophores within cells. From video microscopy of an ensemble of cells, significantly photobleached, we can calibrate fluorescence intensities with respect to fluorophore number without requiring any external calibration. We present three primary results:

1. Integrating over the entire photobleaching time-course, using Eq. 6, improves the resulting quantification. It is natural to do this integral in terms of $p = \exp(-t/\tau)$ the surviving fraction of fluorophores. This gives a cell-by-cell estimate of ν, the proportionality between fluorescence intensity and fluorophore number via $I = \nu n$.
2. We have calculated the errors of ν as a function of the number of initial fluorophores n_0. The results are shown in Eq. 12 and Fig. 3. For accessible $n_0 \gtrsim 10$, the cell-by-cell standard-deviation of ν is approximately constant and given by $\delta\nu/\nu \approx \sqrt{4/5}$. This allows cell-by-cell estimates of ν to be simply averaged, even if n_0 varies widely between cells.
3. We have explored the systematic effects of studying only a finite collection or ensemble of M cells. This leads to a small systematic underestimate of ν, as described by Eq. 14 and shown in Fig. 4, which is typically less than the statistical errors. Furthermore, we have shown that this systematic error can be corrected for—leading to an unbiased estimate of ν even with a finite ensemble of M cells. The statistical errors expected for M cells are $\delta\nu/\nu \approx \sqrt{4/(5M)}$. We have calculated these results, and confirmed them with exact Gillespie simulation of photobleaching.

The principle advantage of our photobleach fluctuation quantification approach over previous division-fluctuation approaches (10,11) is that it can be, in principle, used for nondiffusing fluorophores in nondividing cells of arbitrary geometry. Because many interesting proteins are localized (12) to membranes or organelles, this should greatly expand the utility of these fluctuation-quantification approaches. The photobleaching rate can also be adjusted in comparison to other dynamical processes of the cell such as cell-division or protein synthesis. This allows possible systematic effects due to these other noisy dynamical processes to be explored and avoided. In contrast, division-fluctuations arise after slow septation that cannot be adjusted with respect to protein synthesis rates in the daughter cells. Nevertheless, our analysis of fluctuations is straightforward and can be applied to division-fluctuations—together with our error-analysis of the quantification.

Remarkably, division-fluctuation quantification approaches have not been validated (10,11)—against either internal or external standards. This speaks to the paucity of reliable, accurate, and convenient methods for protein quantification in vivo (1). Although comparison with internal standards (8,9) or with respect to counting individual fluorophores (2,3) are called for, they will not be able to be applied every time. Self-consistency checks are also required. Accordingly, we have presented the expected time-dependence of the average photobleach fluctuations in Eq. 4 and Fig. 2. We have also discussed how, e.g., shot-noise or cell-motion artifacts may be distinguished from photobleaching fluctuations through a consideration of time-dependence and illumination-intensity dependence.

Fluctuation correlation spectroscopy (FCS) can also provide quantification calibration (4). Our photobleach-fluctuation quantification approach exploits temporal fluctuations within an entire cell—where there are no fluctuations due to diffusion into and out of the imaging volume. As a result, we estimate the number of fluorophores in the cell. In contrast, FCS exploits diffusive fluctuations through a small beam-spot—and neglects fluctuations due to relatively slow photobleaching (30). As a result, FCS estimates the average number of fluorophores in the beam-spot. Photobleach-fluctuations provide a complementary quantification approach to FCS, and do not require an independent estimate of the cellular volume.

The immediate challenge is to test our framework experimentally, ideally in comparison with a previously validated quantification approach. Although the timescale of photobleaching can be easily adjusted by the illumination intensity, it remains to be seen whether a practical regime

exists that is slow enough to obtain clear images with respect to background noise sources but fast enough to avoid artifacts due to ongoing protein expression or cellular movement. We also recognize that photobleach photophysics are not well studied for most fluorophores, and one might expect that photobleach environmental sensitivity could vary considerably among, e.g., GFP variants, just as the sensitivity of both brightness and photobleach rates themselves vary (17). To characterize photobleaching fluctuations, the ensemble of cells used must have, on the timescale of photobleaching, similar photophysics. We do not yet know how restrictive this requirement is.

Finally, we note that our analysis of photobleaching fluctuations applies to any superposition of n_0 discrete decaying processes, not just photobleaching of fluorophores. What is needed is single-cell imaging with sufficient dynamic range to resolve both the total cellular signal, $O(n_0)$, and its fluctuations during decay, $O(\sqrt{n_0})$. In practice, optical techniques appear to be the most promising and genetically encoded fluorophores the most convenient.

APPENDIX 1: RAW VARIANCE OF INTENSITIES FOR A DISTRIBUTION OF INITIAL INTENSITIES

Although it is preferable to estimate ν independently for every cell i, using Eq. 6, and then average the resulting ν_i, one might also consider the ensemble of cellular intensities. Given an initial distribution of expression $P_0(n_0)$, then, at a later time characterized by an unbleached fraction p, the distribution of the number n of remaining fluorophores will be given by the convolution

$$P(n) = \sum_{n_0=n}^{\infty} P_0(n_0)\binom{n_0}{n}p^n(1-p)^{n_0-n}, \tag{16}$$

$$= \sum_{n_0=n}^{\infty} P_0(n_0)\binom{n_0}{n}p_A^n p_B^{n_0-n}, \tag{17}$$

where the use of $p_A = p$ and $p_B = 1 - p$ allows us to easily take the first moment

$$\langle n\rangle = \sum_{n=0}^{\infty} P(n)n, \tag{18}$$

$$= p_A\frac{\partial}{\partial p_A}\sum_{n=0}^{\infty} P(n), \tag{19}$$

$$= p_A\frac{\partial}{\partial p_A}\sum_{n_0=0}^{\infty} P_0(n_0)\sum_{n=0}^{n_0}\binom{n_0}{n}p_A^n p_B^{n_0-n}, \tag{20}$$

$$= p_A\frac{\partial}{\partial p_A}\sum_{n_0=0}^{\infty} P_0(n_0)(p_A+p_B)^{n_0}, \tag{21}$$

$$= p\sum_{n_0=0}^{\infty} n_0P_0(n_0), \tag{22}$$

$$= p\langle n_0\rangle, \tag{23}$$

where we used $P_A + P_B = 1$. The variance may be similarly approached

$$\langle n^2\rangle = \sum_{n=0}^{\infty} P(n)n^2, \tag{24}$$

$$= \left(p_A^2\frac{\partial^2}{\partial p_A^2} + p_A\frac{\partial}{\partial p_A}\right)\sum_{n_0=0}^{\infty} P_0(n_0)(p_A+p_B)^{n_0}, \tag{25}$$

$$= \sum_{n_0=0}^{\infty}\left(p^2n_0(n_0-1) + pn_0\right)P_0(n_0), \tag{26}$$

$$= p^2\langle n_0^2\rangle + \left(p-p^2\right)\langle n_0\rangle, \tag{27}$$

so that the number variance is

$$\sigma_n^2 \equiv \langle n^2\rangle - \langle n^2\rangle = \sigma_{n_0}^2p^2 + \langle n_0\rangle p(1-p), \tag{28}$$

which, using $I = \nu n$, directly gives Eq. 8.

APPENDIX 2: CALCULATION OF σ^2_ν DUE TO NUMBER OF FLUOROPHORES

Although integrating fluctuations over p, as in Eq. 6, allows for a better estimate of ν, the accuracy of the estimate is complicated by autocorrelations between fluctuations—as illustrated by the individual traces in Fig. 1. Nevertheless, we can exactly calculate the variance σ^2_ν of the integrated estimate for ν.We start with a single sample with n_0 initial fluorophores. We take the set of ordered photobleach p values to be $\{p_n\}$ with $n \in \{1, 2,\ldots, n_0\}$, where $p_n = \exp(-t_n/\tau)$ corresponds to the time t_n when the system was bleached from n to $n - 1$ fluorophores. We have $p_{n_0} \geq p_{n_0-1} \geq \ldots \geq p_1$. From these photobleach times we can evaluate $\nu_{\{p_i\}}$,

$$\nu_{\{p_i\}} = 6\nu\int_0^1 \left(n(p) - pn_0\right)^2\frac{dp}{n_0}. \tag{29}$$

Because $n(p)$ is piecewise-constant, we then have

$$\int_0^1 (n-pn_0)^2dp = \int_0^{p_1}(0-pn_0)^2dp + \int_{p_1}^{p_2}(1-pn_0)^2dp + \int_{p_{n_0}}^1 (n_0-pn_0)^2dp, \tag{30}$$

$$= \frac{1}{3n_0}\sum_{n=1}^{n_0}\left[(n-p_nn_0)^3 - (n-1-p_nn_0)^3\right], \tag{31}$$

$$= \frac{n_0^2}{3} + n_0 \sum_{n=1}^{n_0} p_n^2 - \sum_{n=1}^{n_0} (2n-1)p_n. \quad (32)$$

To obtain the average contribution, $\nu = \langle \nu_{\{p_i\}} \rangle = I[\nu_{\{p_i\}}]$, we need to average over all possible ordered photobleach times with an ordered integral

$$I \equiv n_0! \int_0^1 dp_{n_0} \int_0^{p_{n_0}} dp_{n_0-1} \ldots \int_0^{p_{j+1}} dp_j \ldots \int_0^{p_2} dp_1. \quad (33)$$

The initial $n_0!$ normalizing factor arises from the uncorrelated (uniform in p) photobleaching of the independent fluorophores, so that $I[1] = 1$. Given an expression that is an integer power a of some p_j, we can obtain its average value

$$I\left[p_j^a\right] = \frac{n_0(n_0-1)\ldots(j)}{(n_0+a)(n_0-1+a)\ldots(j+a)}. \quad (34)$$

We see that $0 \le I[p^a{}_j] \le 1$ and we recover the normalization condition $I[1] = 1$ when $a = 0$. We need $I[p_n] = n/(n_0+1)$ and $I[p^2{}_n] = n(n+1)/[(n_0+1)(n_0+2)]$ to verify that $\nu = \langle \nu_{\{p_i\}} \rangle = I[\nu_{\{p_i\}}]$. We then use $\nu_{\{p_i\}}$ from Eqs. 29 and 32 to calculate the expected variance of $\nu_{\{p_i\}}$:

$$\sigma_\nu^2 \equiv I\left[\left(\nu_{\{p_i\}} - \nu\right)^2\right], \quad (35)$$

$$= I\left[\nu_{\{p_i\}}^2\right] - \nu^2, \quad (36)$$

$$\begin{aligned} =& \frac{36\nu^2}{n_0^2} I\left[\frac{n_0^4}{9} + n_0^2\left(\sum_{n=1}^{n_0} p_n^2\right)^2 + \left(\sum_{n=1}^{n_0}(2n-1)p_n\right)^2 \right. \\ &+ \frac{2n_0^3}{3}\sum_{n=1}^{n_0} p_n^2 - \frac{2n_0^2}{3}\sum_{n=1}^{n_0}(2n-1)p_n \\ &\left. - 2n_0 \sum_{n=1}^{n_0} p_n^2 \sum_{m=1}^{n_0}(2m-1)p_m\right] - \nu^2, \end{aligned} \quad (37)$$

$$\begin{aligned} =& \frac{36\mathrm{v}^2}{n_0^2}\left[\frac{n_0^4}{9} + n_0^2\left(\frac{n_0^2}{9} + 4\frac{n_0}{45}\right) + \frac{2n_0^2}{3}\left(-\frac{n_0^2}{3} + \frac{n_0}{6}\right),\right. \\ =& \left. -2n_0\frac{n_0}{180}\left(40n_0^2 + 6n_0 - 1\right)\right] - \nu^2, \end{aligned} \quad (38)$$

$$= \left[\frac{4}{5} - \frac{3}{5n_0}\right]\nu^2. \quad (39)$$

To evaluate Eq. 37, we have used, where $n \ge m$,

$$I[p_n p_m] = \frac{m(n+1)}{[(n_0+1)(n_0+2)]},$$

$$I\left[p_n^2 p_m^2\right] = \frac{m(m+1)(n+2)(n+3)}{[(n_0+1)(n_0+2)(n_0+3)(n_0+4)]},$$

$$I\left[p_n^2 p_m\right] = \frac{m(n+1)(n+2)}{[(n_0+1)(n_0+2)(n_0+3)]},$$

and

$$I\left[p_n p_m^2\right] = \frac{m(m+1)(n+2)}{[(n_0+1)(n_0+2)(n_0+3)]}.$$

Our final expression, Eq. 39, is the statistical variance of the estimated single-cell ν, and is confirmed with stochastic simulations with various n_0 values in Fig. 3.

We thank Manfred Jericho for discussions, and Slaven Radic for exploratory numerical work.

C.R.N. thanks ACEnet for a postdoctoral fellowship and computational resources, and we thank the Natural Sciences and Engineering Research Council (Canada) for support from their operating grant program.

REFERENCES

1. Wu, J.-Q., C. D. McCormick, and T. D. Pollard. 2008. Chapter 9: Counting proteins in living cells by quantitative fluorescence microscopy with internal standards. *Methods Cell Biol.* 89:253–273.
2. Leake, M. C., J. H. Chandler, …, J. P. Armitage. 2006. Stoichiometry and turnover in single, functioning membrane protein complexes. *Nature.* 443:355–358.
3. Ulbrich, M. H., and E. Y. Isacoff. 2007. Subunit counting in membrane-bound proteins. *Nat. Methods.* 4:319–321.
4. Digman, M. A., C. M. Brown, …, E. Gratton. 2005. Measuring fast dynamics in solutions and cells with a laser scanning microscope. *Biophys. J.* 89:1317–1327.
5. Toomre, D., and J. Bewersdorf. 2010. A new wave of cellular imaging. *Annu. Rev. Cell Dev. Biol.* 26:285–314.
6. Davidson, C. J., and M. G. Surette. 2008. Individuality in bacteria. *Annu. Rev. Genet.* 42:253–268.
7. Rosenfeld, N., J. W. Young, …, M. B. Elowitz. 2005. Gene regulation at the single-cell level. *Science.* 307:1962–1965.
8. Dundr, M., J. G. McNally, …, T. Misteli. 2002. Quantitation of GFP-fusion proteins in single living cells. *J. Struct. Biol.* 140:92–99.
9. Wu, J.-Q., and T. D. Pollard. 2005. Counting cytokinesis proteins globally and locally in fission yeast. *Science.* 310:310–314.
10. Rosenfeld, N., T. J. Perkins, …, P. S. Swain. 2006. A fluctuation method to quantify in vivo fluorescence data. *Biophys. J.* 91:759–766.
11. Teng, S.-W., Y. Wang, …, N. P. Ong. 2010. Measurement of the copy number of the master quorum-sensing regulator of a bacterial cell. *Biophys. J.* 98:2024–2031.
12. Werner, J. N., E. Y. Chen, …, Z. Gitai. 2009. Quantitative genome-scale analysis of protein localization in an asymmetric bacterium. *Proc. Natl. Acad. Sci. USA.* 106:7858–7863.
13. Ormö, M., A. B. Cubitt, …, S. J. Remington. 1996. Crystal structure of the *Aequorea victoria* green fluorescent protein. *Science.* 273:1392–1395.
14. Swaminathan, R., C. P. Hoang, and A. S. Verkman. 1997. Photobleaching recovery and anisotropy decay of green fluorescent protein GFP-S65T in solution and cells: cytoplasmic viscosity probed by green fluorescent protein translational and rotational diffusion. *Biophys. J.* 72:1900–1907.
15. Elowitz, M. B., M. G. Surette, …, S. Leibler. 1997. Photoactivation turns green fluorescent protein red. *Curr. Biol.* 7:809–812.
16. Bogdanov, A. M., E. A. Bogdanova, …, K. A. Lukyanov. 2009. Cell culture medium affects GFP photostability: a solution. *Nat. Methods.* 6:859–860.
17. Shaner, N. C., M. Z. Lin, …, R. Y. Tsien. 2008. Improving the photostability of bright monomeric orange and red fluorescent proteins. *Nat. Methods.* 5:545–551.

18. Gillespie, D. T. 1977. Exact stochastic simulation of coupled chemical reactions. *J. Phys. Chem.* 81:2340–2361.

19. Taniguchi, Y., P. J. Choi, …, X. S. Xie. 2010. Quantifying *E. coli* proteome and transcriptome with single-molecule sensitivity in single cells. *Science.* 329:533–538.

20. Turton, D. A., G. D. Reid, and G. S. Beddard. 2003. Accurate analysis of fluorescence decays from single molecules in photon counting experiments. *Anal. Chem.* 75:4182–4187.

21. Raj, A., and A. van Oudenaarden. 2008. Nature, nurture, or chance: stochastic gene expression and its consequences. *Cell.* 135:216–226.

22. Dickson, R. M., A. B. Cubitt, …, W. E. Moerner. 1997. On/off blinking and switching behavior of single molecules of green fluorescent protein. *Nature*. 388:355–358.

23. Haupts, U., S. Maiti, …, W. W. Webb. 1998. Dynamics of fluorescence fluctuations in green fluorescent protein observed by fluorescence correlation spectroscopy. *Proc. Natl. Acad. Sci. USA*. 95:13573–13578.

24. Berglund, A. J. 2004. Nonexponential statistics of fluorescence photobleaching. *J. Chem. Phys.* 121:2899–2903.

25. Prummer, M., and M. Weiss. 2006. Bulk fluorescence measurements cannot probe the survival-time distribution of single molecules. *Phys. Rev. E.* 74:021115.

26. Rocheleau, J. V., M. Edidin, and D. W. Piston. 2003. Intrasequence GFP in class I MHC molecules, a rigid probe for fluorescence anisotropy measurements of the membrane environment. *Biophys. J.* 84: 4078–4086.

27. Kubitscheck, U., O. Kückmann, …, R. Peters. 2000. Imaging and tracking of single GFP molecules in solution. *Biophys. J.* 78:2170–2179.

28. Soper, S. A., H. L. Nutter, …, E. B. Shera. 1993. The photophysical constants of several fluorescent dyes pertaining to ultrasensitive fluorescence spectroscopy. *Photochem. Photobiol.* 57:972–977.

29. Cannone, F., M. Caccia, …, G. Chirico. 2004. Single molecule spectroscopic characterization of GFP-MUT2 mutant for two-photon microscopy applications. *Microsc. Res. Tech.* 65:186–193.

30. Widengren, J., and R. Rigler. 1996. Mechanisms of photobleaching investigated by fluorescence correlation spectroscopy. *Bioimaging.* 4:149–157.